Industrial Engineering Journal
ISSN: 0970-2555
Volume : 53, Issue 9, September : 2024

Sensorless control of PV Fed BLDC Motor through ANFIS Controller

D. ABHIGNA[1], S. TARA KALYANI[2]
[1]PG Scholar, Department of Electrical And Electronics Engineering, Jawaharlal Nehru technological University Hyderabad, TS, India email: abhidosala@gmail.com
[2]Senior Member, IEEE, Department of Electrical And Electronics Engineering, Jawaharlal Nehru technological University Hyderabad, TS, India email: tarakalyani@gmail.com

Abstract: The main objective of the proposed system is Sensorless control of PV Fed BLDC Motor through ANFIS Controller**.** In this paper, 5- level cascaded Multi-Level Inverter (MLI) with Adaptive neuro fuzzy inference system (ANFIS) controller for speed range position sensorless control of solar photovoltaic array fed PM BLDC motor drive is proposed. An elimination of position sensor and current sensor for rotor position estimation makes the implemented drive compact and cost effective for agricultural application Through simulation and laboratory testing, the compact and cost-effective ANFIS-controlled drive demonstrates reliability, making it an ideal solution for affordable and efficient agricultural applications, catering to both irrigation and domestic water pumping needs. Using MATLAB software the outputs of the solar PV array and BLDC motor are validated in the two conditions at steady state and dynamic state.

Key Words — Incremental Conductance (INC) Maximum Power Point Tracking (MPPT) algorithm,Permanent Magnet Brushless Direct Current (PMBLDC) Motor Drive, Position Sensorless control, Mulitlevel inverter, ANFIS Controller

I.INTRODUCTION

The Since solar photovoltaic (PV) arrays have grown significantly less expensive and fossil fuels are running out quickly, solar energy has emerged as one of the most reliable nonrenewable energy sources. Water pumping is critically needed since the lack of water is having a severe impact on agriculture and the availability of drinkable water, particularly during the summer in rural areas of India and other low-lying regions of the world. The environment is polluted and diesel-energized pumps have ongoing operating costs. Their significance is diminishing as water pumps powered by solar PV arrays, particularly for irrigation, become more significant. The motor-coupled water pumps have also replaced hand pumps that provide drinkable water in rural regions these days. Water pump powered by solar photovoltaic cells, permanent magnet brushless DC. A water pumping motor drive application, known as PMBLDC, is provided [1] .But the solar-powered water pump with a DC motor connected can operate without a drive directly. But they're constantly having problems with commutator brushes that need maintenance. Since induction motors require very little maintenance, they can be used extensively, but their middling efficiency raises the solar panel's rating, which raises the system's cost [2]–[4]. Because Hall effect sensors are sensitive to temperature, there is a significant risk of sensor failure during severe weather, rendering the system unstable. Therefore in order to overcome these issues, For both surface-mounted and submerged BLDC motor-based irrigation pumps, it is preferable to switch to position sensor-less control. [5] presents an efficient zero-speed startup with position sensor-free PMBLDC motor drive control. A trustworthy speed range position estimate function is provided here to start the motor from the stall state to the high speed range. In [6] and [7], the rotor starting position calculation is performed using an estimate of the Inductance of stator winding. The location of the rotor and stator core saturation information affect the inductance. The reverse electromotive force (EMF) zero crossover is detected using a resistor and a cascaded low-pass filter (LPF). By using torque estimates as a reference for rotor location and back EMF and rotor speed to estimate torque constant, position sensor-less control has been accomplished in [8] [10]. The irrigation water pump is driven by a PM-BLDC motor fed by a solar photovoltaic array through a wide speed range position sensor-less control algorithm based on peak current detection. The

Industrial Engineering Journal
ISSN: 0970-2555
Volume : 53, Issue 9, September : 2024

precise beginning commutation and peak staring current are controlled by this starting algorithm. Because it doesn't need a position sensor or a current sensor, the developed drive for rotor position estimation is small and affordable for agricultural use. Advanced technology is widely available for water pumping systems that are powered by solar PV and brushless DC motors. Proposed is the BLDC motor supplied aqua pumping system with A neuro-fuzzy inference system that is adaptable (ANFIS). The ANFIS controller combines fuzzy and neural systems. Here, a controller is utilized as a high stepup maximum power point tracking, or MPPT, is controlled by the inverter. by an ANFIS-based effective particle swarm incremental conductance (INC) method. An aqua pumping brushless dc motor with a soft start feature and a buck boost converter arrangement is shown in [12]. An INC approach with a buck boost converter was used to realize the MPPT. From the perspective of power electronics, this simplifies the system. However, because of reliability and cost-effectiveness issues, the system— which includes a position sensor—is not commonly accepted. Water pumping with solar PV has been shown using ANFIS controller-based MPPT implemented drives. Comparing an ANFIS controller-based MPPT to a fuzzy logic controller, it has been observed that the total system efficiency is increased. It is mentioned in [15] that a PMBLDC motor's position sensorless control has been enhanced during startup. The sensing circuit, which is based on an analog comparator, is not appropriate for submersible applications or for pumping. A BLDC motor drive coupled to an Multilevel Inverter has been presented for water pumping. System efficiency has increased as a result of the intermediate converter being removed because the multilevel inverter handles both motor commutation and MPPT.

II. PROPOSED SYSTEM

In existing system, a single-stage position sensorless control of the PMBLDC motor drive for surface mounted as well as submersible water pumping, especially for irrigation applications. The proposed model has PV panel, multilevel inverter, the electronic commutator and the PMBLDC motor shown fig.1. The ANFIS controller is used as the controller in this system. The input given to the solar panel is in irradiance (w/m2). The input provided at the PV panel gives DC current. So the Dc current need to convert as AC current. The inverter is used for the convert from DC to AC. Multilevel inverter is used in the proposed model. An output that uses a voltage source inverter settles more slowly. A multilevel inverter can reduce the output's settling time when it replaces the voltage source inverter. By using the multilevel inverter the efficiency of the system is increased so power quality also increased.

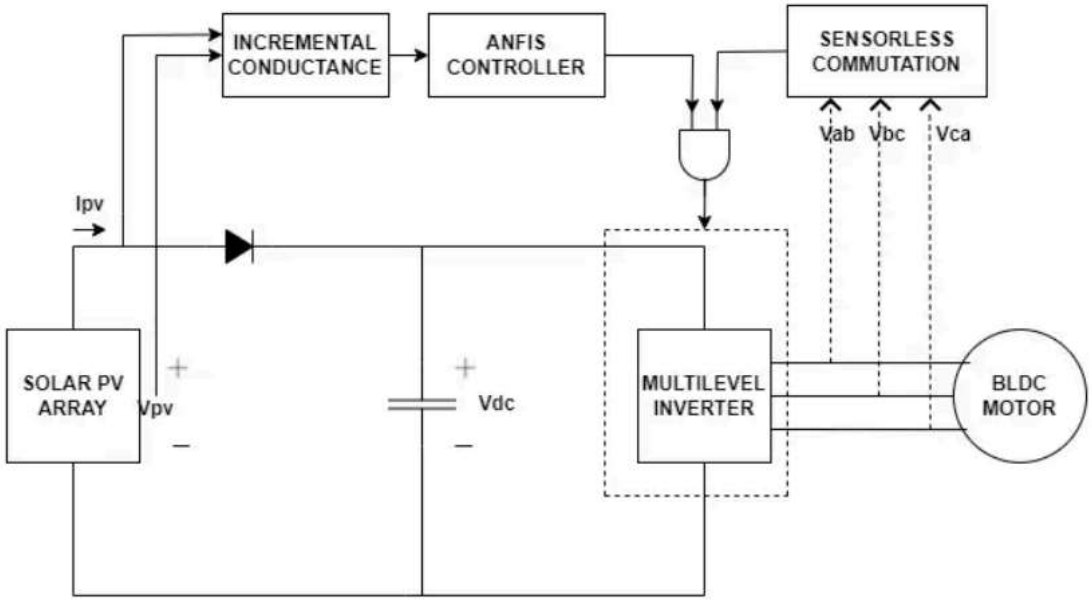

Fig. 1. Proposed System configuration of position sensorless brushless dc motor drive.

III. MATHEMETICAL MODELLING

The proper design of a PV array plays an important role for the BLDC motor drive based water pump. A 3000-r/min, 4-pole, 1.3-kW BLDC motor is considered. The system is designed in such a way that with the rapid variation of solar insolation, the system maintains the minimum speed. Detailed specifications of brushless dc motor are given in Table I.

PARAMETERS	RATINGS
Power	1.3KW
Speed	3000rpm
Pole number	4
Resistance of winding	2.1 ohm
Inductance	9.13Mh
Moment of inertia	0.29Kg/m
Motor torque constant	68V/Krpm
Motor voltage constant	0.74m/A

A. Solar PV Array Sizing

For the steady-state optimum performance, a solar irradiance of 1000 W/m2 is considered at standard test condition [17]. Though the the motor power rating is 1.3 kW but the power rating of the solar PV array is considered as 1.5 kW to fulfill the system's intermediate losses. The voltage of PV array is considered 310 V at full load at 1000 W/m2 irradiance. The estimation of capacitor C is carried out as

$$C = \frac{I_{dc}}{6\times\omega\times\Delta V_{dc}} \qquad (1)$$

$$I_{dc} = \frac{P_{mpp}}{V_{dc}} = \frac{1500}{310} = 4.83A;\ I_{dc} = dclink\ current$$

$$\omega = \frac{2\times\pi\times N}{60} = \frac{2\times\pi\times3000}{60} = 314.159\frac{rad}{s};$$

N=motor speed for water pumping = 3000 r/min. ΔV_{dc}=dc-link ripple voltage, and it is considered as 2% of Vdc; therefore, the dc-link capacitance is estimated as

$$C = \frac{I_{dc}}{6\times\omega\times\Delta V_{dc}} = \frac{4.83}{6\times314.159\times0.02} = 500\mu F.$$

As the dc-link voltage is having sixth harmonic component of the VSI output voltage, it is finally selected as $C = 470mF$.

B. Cascaded H-bridge MLI

Fig.2 shows a five level cascaded H-bridge multilevel inverter. The converter consists of two series connected H-bridge cells which are fed by independent voltage sources. The outputs of the H-bridge cells are connected in series such that the synthesized voltage waveform is the sum of all of the individual cell outputs. The output voltage is given by

$$V = V_1 + V_2 \qquad (2)$$

Where the output voltage of the first cell is labeled V1 and the output voltage of the second cell is denoted by V2.There are five level of output voltage i.e 2V, V, 0, -V, -2V.The main advantages of cascaded H-bridge inverter is that it requires least number of components, modularized circuit and soft switching can be employed. But the main disadvantage is that when the voltage level increases, the number of switches increases and also the sources, this in effect increases the cost and weight. The cascaded H-bridge multilevel inverters have been applied where high power and power quality are essential, for example, static synchronous compensators, active filter and reactive power compensation applications, photo voltaic power conversion, uninterruptible power supplies, and magnetic resonance imaging. Furthermore, one of the growing applications for multilevel motor drive is electric and hybrid power trains.

Industrial Engineering Journal
ISSN: 0970-2555
Volume : 53, Issue 9, September : 2024

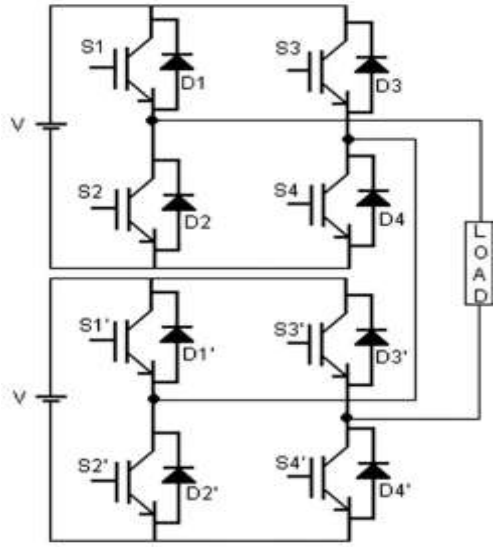

Fig.2. Five level cascaded H-bridge multilevel inverter

IV. CONTROL STRATAGY

A. Position Sensorless Control

The commutation position in the BLDC motor is the switching time when the back EMF of the inbound phase equals the outgoing phase back EMF. The back EMF of the incoming phase at the time of commutation attains the maximum value, and outgoing phase's back EMF starts decreasing from its maximum value. At the exact commutation point, the values of incoming and outgoing phase back EMF are the same and the back EMF of the line is zero and just changed to positive from negative and vice versa. In the case of a BLDC motor, two phases conduct simultaneously and one phase remains floated. At each and every 60° interval, one conducting phase is switched off and one floating phase is switched on. Considering the switching of conduction from a-c to b-c phases, just beginning of the commutation, the current through phase a is not changing and through phase b is zero, i.e., ia = I and ib = 0, and after the instant current through phase b is fixed and through phase a is zero, i.e., ia = 0 and ib = I. For a whole cycle of switching, there is no voltage drop across the inductor as the average current through it has not changed as it can be explained by the following equations. Phase a and phase b voltages are given by the following equations at the starting of the commutation:

$$v_{an} = Ri_a + e_a;\ v_{bn} = e_b \quad (3)$$

Thus, the line voltage is given as

$$v = Ri_a + (e_a - e_b); \quad (4)$$

The voltage of line becomes zero at the time commutation and neglecting the Ria drop, directly gives the ideal commutation instant, that is ea = eb, considering (3), which reduces to

$$e_a = e_b\ ,\ v_{an} = v_{bn} \quad (5)$$

As the line back EMFs are not directly accessible, in this method, by neglecting winding resistance drop, the line voltage is taken directly instead of line back EMFs. The line voltages can be simply measured at themotor terminals. The line voltage zero crossing point is taken as commutation instant. This mentioned control scheme is described in Fig. 3.

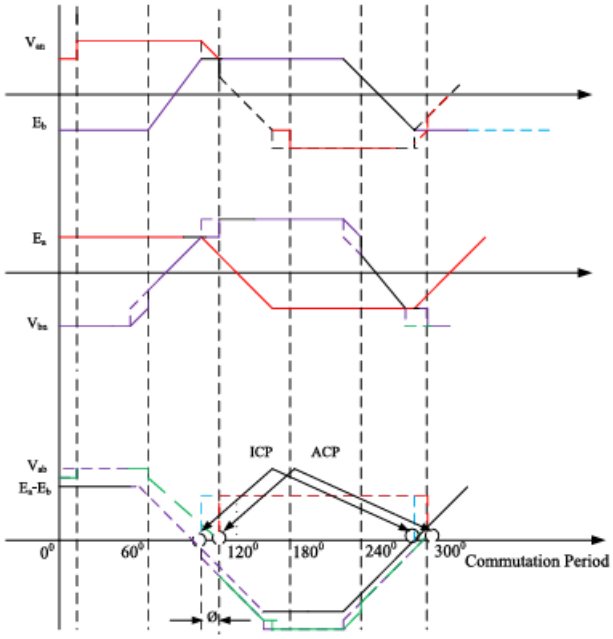

Fig. 3. Estimation of commutation point from back EMF

B. Control of Maximum Power Point

The INC [19] based MPPT control is applied to extract the maximum power by operating the intermediate converter at solar optimum operating point from a solar PV array. The INC-based algorithm determines the direction of perturbation according to the slope of the solar P-V characteristics. The flow diagram is elaborated in

Industrial Engineering Journal
ISSN: 0970-2555
Volume : 53, Issue 9, September : 2024

Fig. 4. According to this algorithm, the slope of the mentioned curve is zero at MPP. It is positive when it is on the left and it is negative when it is on the right. This operation is described in the following equations:

$\frac{dP_{pv}}{dv_{pv}}$ = 0, at maximum power point (6)

$\frac{dP_{pv}}{dv_{pv}}$ > 0, when optimum operating point is at the left (7)

$\frac{dP_{pv}}{dv_{pv}}$ < 0, when optimum operating point is at the right. (8)

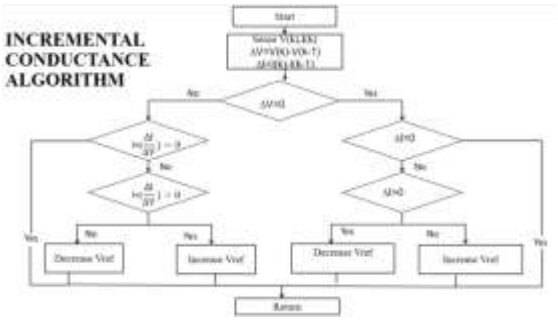

Fig. 4. State flow of incremental conductance method.

C. Design of Low-Pass Filter

The line voltages sensed for position sensorless commutation estimation contain unwanted commutation ripple due to freewheeling diode conduction. The phase back EMFs estimated from line voltages also contain some ripples and high frequency switching components of the line voltage. This ripple content causes false zero detection and leads to an improper electronic commutation during sensorless position estimation process. The high frequency component and spike are eliminated for proper position estimation and electronic commutation using first-order LPF. For LPF design, the selection of proper cutoff frequency is very important. A low cutoff frequency of the LPF causes high phase lag to the system, whereas high cutoff frequency causes high frequency component to be present in the filtered signal, which again causes improper position detection and wrong commutation switching. For this application, the rated system frequency is 100 Hz as the motor rated speed is 3000 r/min.

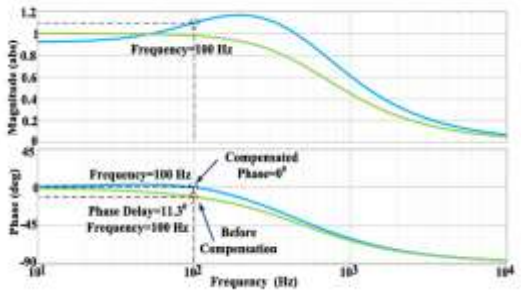

Fig. 5. Magnitude and phase plot after compensation in phase.

The cutoff frequency of the LPF is determined in such a way that neither very low cutoff frequency creates high phase lag in the system nor the high cutoff frequency passes high frequency component. Using a detailed control analysis and Bode plot, the cutoff frequency of the LPF is determined as 500 Hz. The corresponding Bode plot is shown in Fig. 5. The respective transfer function is determined as

$$H_1(s) = \frac{\omega_c}{s+\omega_c} = \frac{3141.6}{s+3141.6} \quad (9)$$

Where ω_c = filter cutoff frequency, rad/s. For commercial implementation of the PMBLDC motor drive, the designed filter is digitally implemented. For digital implementation of the LPF, the sensed line voltages are sampled at 19.2 kHz and the above transfer function (10) is converted in discrete z-domain [20]. The corresponding z-domain function is

$$H_1(z) = \frac{0.09337}{z-0.9066} \quad (10)$$

From the Bode plot shown in Fig. 5, it is seen that the LPF adds 11.3° phase lag in the system. To compensate the above phase lag and to detect the proper sensorless position, the phase compensator is added in the system.

D. Phase Compensator Design

The phase lead compensator is designed and introduced in the system to compensate the phase lag introduced by the LPF in the system. It is seen from Bode plot in Fig. 5 that 11.3° phase lag is introduced by the LPF. This lag in the estimated back EMFs causes an error in commutation, which creates high ripple in the torque and peaky current. The peaky phase current reduces the lifespan of the stator windings due to extra heating. The commutation error increases according to the increase of the motor

Industrial Engineering Journal
ISSN: 0970-2555
Volume : 53, Issue 9, September : 2024

speed. So the phase lag compensator is very much needed for proper phase compensation. The detailed designs of the phase lead compensator and digital implementation are discussed in[17].The phase compensator transfer function is as follows;

$$G(s) = k\frac{s+\omega_1}{s+\omega_2} \quad (11)$$

where ω1and ω2 are the zero crossover and phase crossover frequency and k is the magnitude constant.

From the Bode plot shown in Fig.5, the phase lag angle = 11.30.The magnitude constant k is determined as

$$k = \frac{1+sin\theta}{1-sin\theta} \quad (12)$$

The phase crossover frequency is calculated as

$$\omega_1 = \frac{1}{kT}, \omega_2 = \frac{1}{T} \quad (13)$$

where T is the time constant. The phase compensator transfer function is

$$G(s) = 1.487\frac{s+515.25}{s+766.189} \quad (14)$$

For digital implementation of the phase compensator in the digital signal processor (DSP), the above transfer function (14) is converted into discrete time domain using Tustin approximation and 19.2-kHz sampling rate

$$G(z) = \frac{1.42z-1.37}{z-0.9545} \quad (15)$$

V. PROPOSED ANFIS CONTROLLER

An Adaptive Neuro-Fuzzy Inference system or adaptive network-based fuzzy inference system (ANFIS) is a kind of artificial neural network that is based on Takagi–Sugeno fuzzy inference system. The technique was developed in the early 1990s.Since it integrates both neural networks and fuzzy logic principles; it has potential to capture the benefits of both in a single framework. Its inference system corresponds to a set of fuzzy IF–THEN rules that have learning capability to approximate nonlinear functions [8, 9, and 11]. Hence, ANFIS is a universal estimator. For using the ANFIS in a more efficient and optimal way, one can use the best parameters obtained by genetic algorithm. It has uses in intelligent situational aware energy management system.

In Fig.6 shows the proposed ANFIS based control architecture. The node functions of each layer in ANFIS architecture are described as follows:

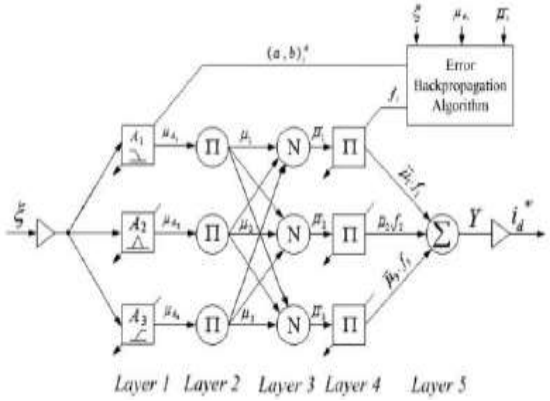

Fig.6. Schematic of the proposed ANFIS

The error between reference dc-link voltage and accurate dc-link voltage (ξ=Vdc*-Vdc) is given to the neuro-fuzzy controller and a similar error is utilized to tune the precondition and ensuing parameters . The control of dc-link voltage gives the active power current segment (id *'), which is additionally adjusted to measure active current part injected from RES (iRen).

Layer 1: This layer is fuzzification layer. Degrees of membership functions are calculated in this layer for each input variable. The input variables of ANFIS are chosen as the error (e) and the change of error (Δe). The trapezoidal and triangular enrolment capacities are utilized to lessen the calculation error as appeared in Fig. 7, the relating node conditions are as given below:

$$O_i^1 = \mu_{Ai}(x) = \frac{1}{1+\left[\left(\frac{x-c_i}{a_i}\right)^2\right]^{bi}} \quad (16)$$

Where x is the input to node i, Ai is the linguistic variable associated with this node function μ_{Ai} is the membership function of Ai, and $\{a_i, b_i, c_i\}$ is the premise parameter set.

Industrial Engineering Journal
ISSN: 0970-2555
Volume : 53, Issue 9, September : 2024

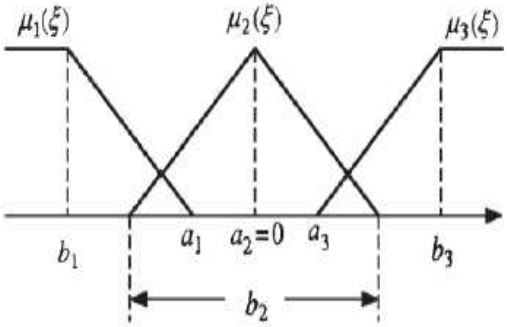

Fig.7. Fuzzy membership functions.

Layer 2: This layer is rule inference layer. Every node in this layer is a fixed node labelled as ∏ which multiplies the incoming signals and sends the product out. Each node output corresponds to the firing strength of a fuzzy rule.

$$O_i^2 = \mu_i = \mu(x)\mu(y) \qquad i = 1,2,3 \qquad (17)$$

Layer 3: This layer is normalization layer. Every node in this layer is a circle node labelled N. The i-th node calculates the ratio of the rule's firing strength to the sum of all rules' firing strength.

$$O_i^3 = \overline{\mu_i} = \frac{\mu_i}{\mu_1+\mu_2+\mu_3} \qquad i = 1,2,3 \qquad (18)$$

Layer 4: This layer is consequent layer. All nodes are an adaptive mode with node function

$$O_i^4 = \overline{\mu_i}.f_i = \overline{\mu_1}(a_0^i + a_1^i\epsilon) \;\; i = 1,2,3 \qquad (19)$$

where wi is the output of Layer 3 and (a_0, a_1) is the consequent parameter set.

Layer 5: This layer is output layer. The single node in this layer is a fixed node labelled ∑ that computes the overall output as the summation of all incoming signals

$$O_i^5 = \mu_i = \sum_i \overline{\mu_i} f_i \qquad i = 1,2,3 \qquad (20)$$

The parameters of ANFIS are updated using the back propagation error term as follow:

$$\frac{\partial E}{\partial O^5} = k_1.e + k_2.\Delta e \qquad (21)$$

The input signals error (e) and the change of error (Δe) multiplied by the coefficients k1 and k2.

$$\alpha_{k+1} = \alpha_k - n\frac{\partial E}{\partial \alpha_k} \qquad (22)$$

where α is any of the parameters of ANFIS and η is learning rate. The error will be reduced next training iteration.

VI. SIMULATION RESULTS

A) EXISTING RESULTS

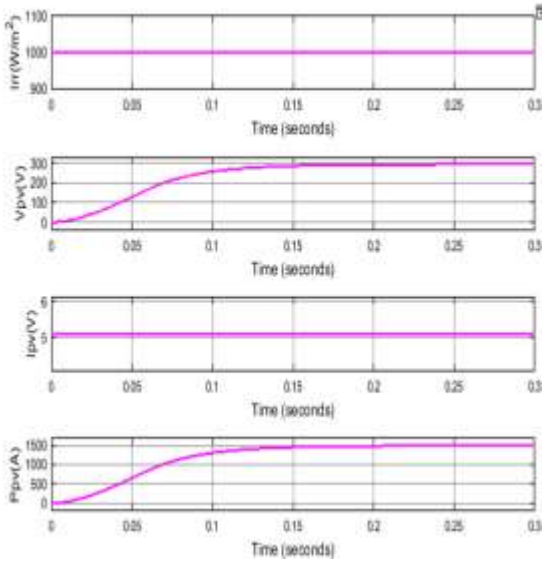

Fig. 8. Steady-state and starting Solar PV array performance of Solar PV array performance at 1000 W/m2 insolation.

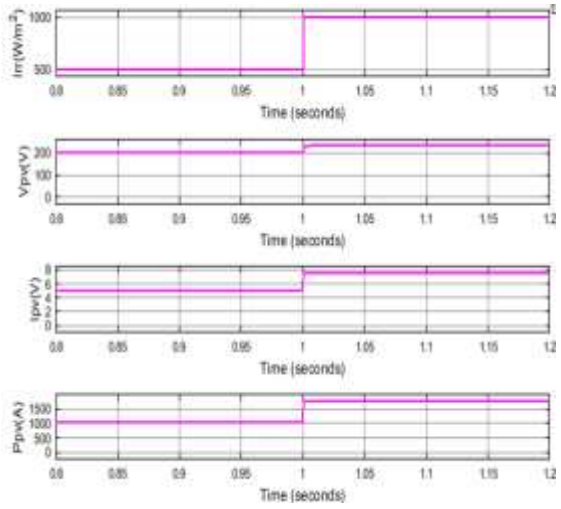

Fig.9. Dynamic performance of Solar PV array varying from 500 to 1000 W/m2.

Industrial Engineering Journal
ISSN: 0970-2555
Volume : 53, Issue 9, September : 2024

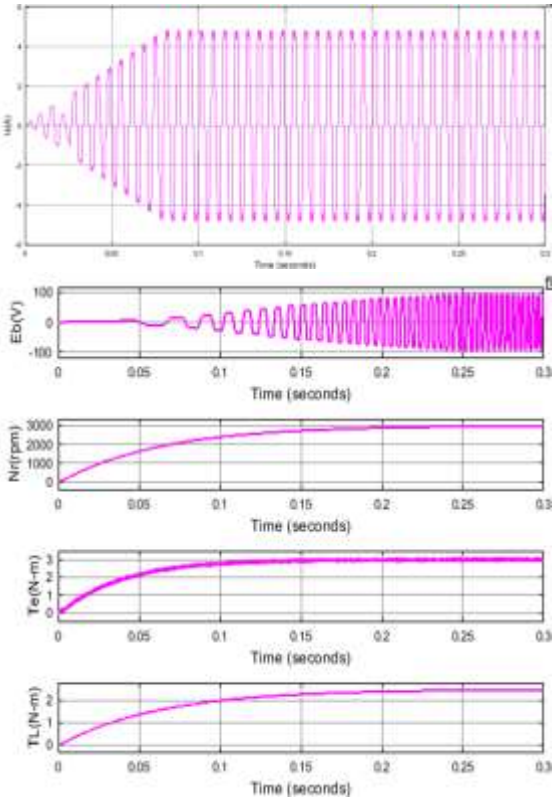

Fig. 10.steady-state performance of BLDC motor at sensorless scheme at 1000 W/m2 irradiance

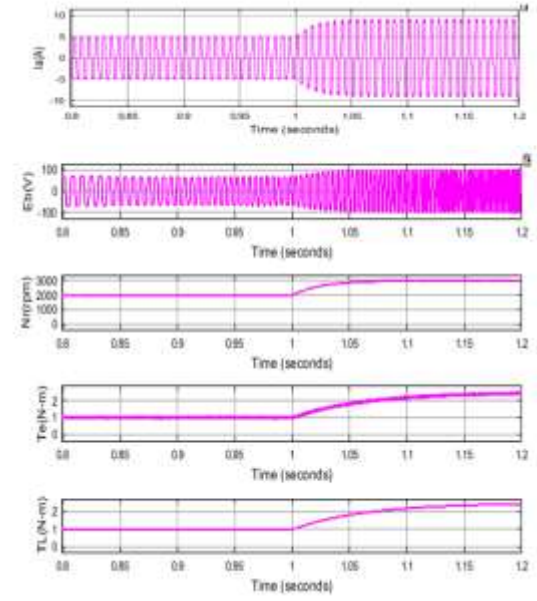

Fig.11. Dynamic performance of BLDC motor at sensorless scheme varying from 500 to 1000 W/m2 irradiance.

B) EXTENSION RESULTS

Performance of an INC MPPT algorithm with ANFIS controller is evaluated at insolation level of 1000 W/m2. A perfect tracking is observed even in dynamically varying weather condition as shown in Fig. 12 and 14. It is seen that the system is having negligible oscillations due to very low perturbation size (0.005) and the initial slow tracking is observed, which allows a soft starting of the BLDC motor. The parameters are evaluated by varying the insolation level from 500 to 1000 W/m2. It is evaluated that the motor attains a speed of 3000 r/min at lower insolation level, which is sufficient for water pumping.

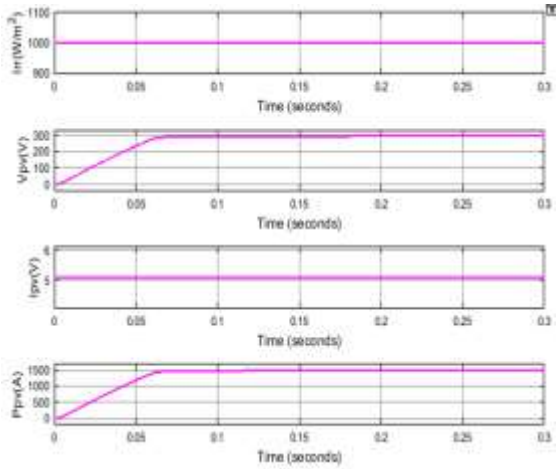

Fig.12. Steady-state and starting Solar PV array performance of Solar PV array performance at 1000 W/m2 insolation.

Industrial Engineering Journal
ISSN: 0970-2555
Volume : 53, Issue 9, September : 2024

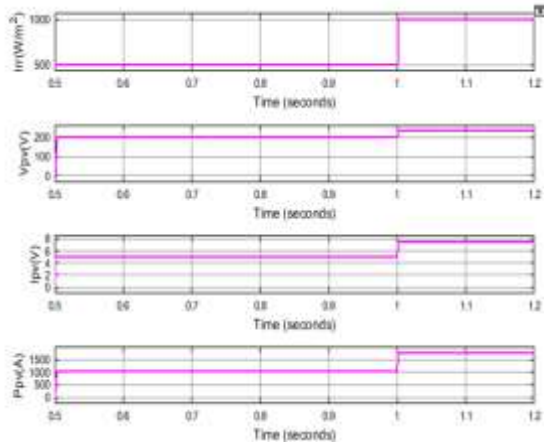

Fig.13. Dynamic performance of Solar PV array varying from 500 to 1000 W/m2.

Starting and steady-state performances of the sensorless BLDC motor for the system are evaluated at 1000 W/m2 irradiance. The dynamic behavior of the system is evaluated at varying insolation levels of 500−1000W/m2 as shown in Fig. 13 and 15. Starting and steady-state performance parameters of the BLDC motor, i.e., the stator phase current (Ia), the back EMF, Eb, the speed, N, backEMF after filtering for sensorless position estimation are evaluated. From the steady-state performance parameters, it is seen that the motor speed is 3000 r/min, which is the optimum speed with maximum efficiency.

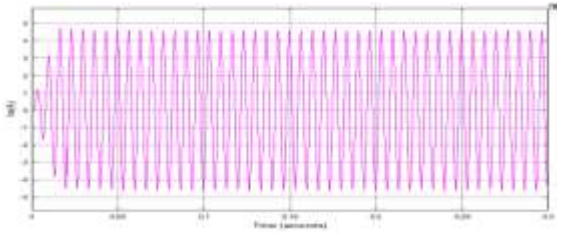

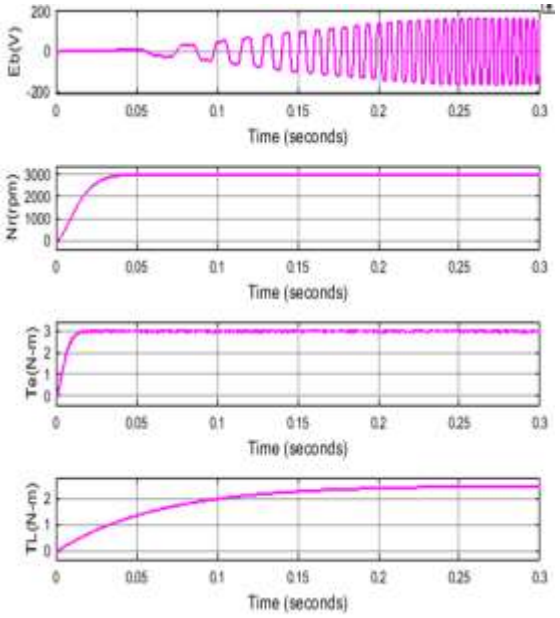

Fig.14. steady-state performance of BLDC motor at sensorless scheme at 1000 W/m2 irradiance

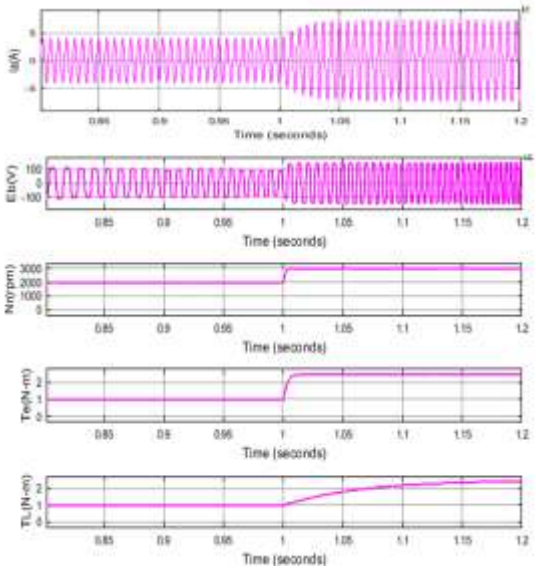

Fig.15. Dynamic performance of BLDC motor at sensorless scheme varying from 500 to 1000 W/m2 irradiance.

CONCLUSION

Sensorless control of PV Fed BLDC Motor through ANFIS Controller is proposed. The robust position sensorless control system is implemented for a PMBLDC motor in solar-powered system, This method ensures an extended lifespan the PMBLDC

motor. By minimizing the reliance on position sensors, the system achieves compactness and cost-effectiveness, while the performance of the solar MPPT and PMBLDC motor are validated through MATLAB/SIMULINK at constant and variable irradaince. With an ANFIS controller, the system exhibits fast settling and stable dynamic performance, ensuring reliable and effective operation.

REFERENCES

[1] A. Sen and B. Singh, "Peak current detection starting based position sensorless control of BLDCmotor drive for PV array fed irrigation pump," in Proc. IEEE Int. Conf. Environ. Elect. Eng. Ind. Commercial Power Syst. Europe (EEEIC /I&CPS Europe), 2019, pp. 1–6.

[2] S. Jain, A. K. Thopukara, R. Karampuri, and V. T. Somasekhar, "A single-stage photovoltaic system for a dual-inverter-fed open-end winding induction motor drive for pumping applications," IEEE Trans. Power Electron., vol. 30, no. 9, pp. 4809–4818, Sep. 2015.

[3] L. An and D. D. Lu, "Design of a single-switch DC/DC converter for a PV-battery-poweredpumpsystem withPFM+PWMcontrol," IEEE Trans. Ind. Electron., vol. 62, no. 2, pp. 910–921, Feb. 2015.

[4] J. V. M. Caracas, G. d. C. Farias, L. F. M. Teixeira, and L. A. d. S. Ribeiro, "Implementation of a high-efficiency, high-lifetime, and low-cost converter for an autonomous photovoltaic water pumping system," IEEE Trans. Ind. Appl., vol. 50, no. 1, pp. 631–641, Jan./Feb. 2014.

[5] T.-H. Kim and M. Ehsani, "Sensorless control of the BLDC motors from near-zero to high speeds," IEEE Trans. Power Electron., vol. 19, no. 6, pp. 1635–1645, Nov. 2004.

[6] S. Dusmez, A. Khaligh, M. Krishnamurthy, E. Ugur, and M. Uzunoglu, "Sensorless control of BLDCs for all speed ranges with minimal components," in Proc. Inter. Aegean Conf. Elect. Machines Power Electron. Electromotion, Joint Conf., 2011, pp. 626–631.

[7] J. Park, S. Hwang, and J. Kim, "Sensorless control of brushless DCmotors with torque constant estimation for home appliances," IEEE Trans. Ind. Appl., vol. 48, no. 2, pp. 677–684, Mar./Apr. 2012.

[8] J. Feng, K. Liu, andQ.Wang, "Scheme based on buck-converter with threephase H-bridge combinations for high-speed BLDC motors in aerospace applications," IET Electric Power Appl., vol. 12, no. 3, pp. 405–414, Mar. 2018.

[9] A. Ahfock and D. Gambetta, "Sensorless commutation of printed circuit brushless direct current motors," IET Electric Power Appl., vol. 4, no. 6, pp. 397–406, Jul. 2010.

[10] R. Kumar and B. Singh, "Buck-boost converter fed BLDC motor drive for solar PV array based water pumping," in Proc. IEEE Inter. Conf. Power Electron., Drives Energy Syst. (PEDES), 2014, pp. 1–6.

[11] G. N. A. Maranhão, A. U. Brito, J. T. Pinho, J. K. S. Fonseca, A. M. Leal, and W. N. Macêdo, "Experimental results of a fuzzy controlled variablespeed drive for photovoltaic pumping systems: A review," IEEE Sensors J., vol. 16, no. 9, pp. 2854–2864, May 2016.

[12] B. Singh and R. Kumar, "Simple brushless DC motor drive for solar photovoltaic array fedwater pumping system," IET Power Electron., vol. 9, no. 7, pp. 1487–1495, 2016.

[13] S. Sheik Mohammed, D. Devaraj, and T. P. Imthias Ahamed, "Maximum power point tracking system for stand alone solar PV power system using adaptive neuro-fuzzy inference system," in Proc. Biennial Inter. Conf. Power Energy Syst.: Towards Sustain. Energy (PESTSE), 2016, pp. 1–4.

[14] A. Gupta, P. Kumar, R. K. Pachauri, and Y. K. Chauhan, "Performance analysis of neural network and fuzzy logic based MPPT techniques for solar PV systems," in Proc. 6th IEEE Power India Inter. Conf. (PIICON), Delhi, India, 2014, pp. 1–6.

[15] K. Lee, D. Kim, B. Kim, and B. Kwon, "A novel starting method of the surface permanent-magnet BLDC motors without position sensor for reciprocating compressor," IEEE Trans. Ind. Appl., vol. 44, no. 1, pp. 85–92, Jan./Feb. 2008.

[16] R. Kumar and B. Singh, "Single stage solar PV fed brushless DC motor driven water pump," IEEE J. Emerg. Sel. Top. Power Electron., vol. 5, no. 3, pp. 1377–1385, Sep. 2017.

[17] W. Bolton, Instrumentation and Control Systems. Oxford, U.K.: Elsevier,2015